Numerical Simulation of Jet Injection and Species Mixing under High-Pressure Conditions

2017 J. Phys.: Conf. Ser. 821 012020

(http://iopscience.iop.org/1742-6596/821/1/012020)

IOP Conf. Series: Journal of Physics: Conf. Series **821** (2017) 012020 doi:10.1088/1742-6596/821/1/012020

Numerical Simulation of Jet Injection and Species Mixing under High-Pressure Conditions

Aswin Gnanaskandan[1] and Josette Bellan[1,2]
[1]California Institute of Technology, Pasadena, CA 91125
[2]Jet Propulsion Laboratory, California Institute of Technology, CA 91109
E-mail: Josette.Bellan@jpl.nasa.gov

Abstract. Direct Numerical Simulation (DNS) and Large Eddy Simulation (LES) are performed of a round fluid jet entering a high-pressure chamber. The chemical compositions and temperatures of the jet and that of the fluid in the chamber are initially prescribed. The governing equations consist of the conservation equations for mass, momentum, species and energy, and are complemented by a real-gas equation of state. The fluxes of species and heat are written in the framework of fluctuation-dissipation theory and include Soret and Dufour effects. For more than two species, the full mass diffusion and thermal diffusion matrices are computed using high-pressure mixing rules which utilize as building blocks the corresponding binary diffusion coefficients. The mixture viscosity and thermal conductivity are computed using standard mixing rules and corresponding states theory. To evaluate the physical model and numerical method, LES is employed first to simulate a supercritical N_2 jet injected into N_2. Time averaged results show reasonable agreement with the experimental data. Then, DNS is conducted to study the spatial evolution of a supercritical N_2 jet injected into CO_2. Time averaged results are used to compute the length of the potential core and the species diffusion characteristics. Spectral analysis is then applied on a time series data obtained at several axial locations and a dominant frequency is observed inside the potential core.

California Institute of Technology, Pasadena, CA 91125, USA

E-mail: `Josette.Bellan@jpl.nasa.gov`

1. Introduction

Numerous propulsion devices - diesel, rocket, gas turbine and HCCI engines - rely on mixing and combustion of chemical species under high-pressure conditions. What distinguishes high-pressure (high-p) fluid behavior from its low-pressure counterpart is the nature of the molecular interactions; under high-p the molecules are much tightly packed and may experience van der Waals interactions and caging effects. Macroscopically, this means that the perfect gas equation of state (EOS) is no longer appropriate to describe this fluid and should be replaced by a real-gas EOS. Moreover, under high-p conditions the fluxes of mass and heat must assume their full form given by the fluctuation-dissipation theory [1], that includes Soret and Dufour effects. For multi-species situations the mass diffusion and thermal diffusion matrices must be fully populated to account for interactions among species rather than interactions between species or interactions of one species with its global complement in the mixture. Clearly, simulating such flows requires complex models. Evaluating such models and simulations with experimental data is crucial in order to gain confidence that the model captures the essential aspects of the situation and

that the numerical method is appropriate. Despite the definite interest in understanding multi-species situations, experimental data for only single and binary species exist so far. Selected representative experimental studies are those of Oschwald and Schik [2] and Meyer et al. [3] who obtained data for N_2-into-N_2 injection; Oschwald et al. [4] who performed experiments with N_2 injection into H_2; Chehroudi et al. [5] who injected N_2 into N_2, O_2, He or a 50%/50% mixture of CO and N_2; Segal and Polikhov [6], Roy and Segal [7] and Roy et al. [8] all of whom obtained data for a fluoroketone jet injected into N_2; and Falgout et al. [9, 10] who observed the injection of n-dodecane in air containing 21% O_2, and butanol, n-dodecane and n-hexadecane in N_2, respectively. No experiments with multi-species (i.e. more than two species) mixing exist, except those of Manin et al. [11] for n-heptane, n-dodecane and n-hexadecane injected into a hot fluid mixture resulting from the burning of C_2H_2 and H_2 in air, but the percent composition of this mixture is not documented although it can generally be assumed to be of H_2O, CO_2 and N_2 in unknown proportions. Most experimental observations are of visual type trying to unravel the species-specific conditions separating the single-phase and two-phase regimes. Quantitative data for validation are rare and restricted to few studies. We ask here whether the available data is sufficient to validate models, i.e. distinguish between the predictions of models that are different and indicate the model which best represents the physics. Failing to do would mean that experimental data of different type than one acquired so far must be obtained, and would open up the discussion regarding which data would be appropriate for model evaluation and whether the diagnostics to acquire this data in an incontrovertible way are available. Among the above-cited investigations, we are particularly interested in the data of Mayer et al. [3] for N_2-into-N_2 injection and of forthcoming data for N_2 injected into CO_2. This last case is partially relevant to engines using exhaust gas re-circulation and of paramount importance for understanding conditions encountered by a lander on Venus.

This paper is organized as follows: First, the previously derived governing equations in the most general form [12] are described, and we refer to other publications for the detailed computation of transport properties. Then, we conduct both LES to evaluate the model by comparison with experimental data and DNS to understand the details of flow evolution in a spatial configuration rather than the temporal configuration of the past [12]. Model evaluation must be necessarily conducted in a spatial rather than temporal realm. Since all our previous studies (e.g. [12]) were performed in the context of a temporal mixing layer, the configuration, numerical method and boundary conditions including inflow conditions are described in detail. The description and analysis of the results follows. A summary and conclusions are finally offered.

2. Description of the governing equations

The governing equations are the conservation equations - continuity, momentum, species and total energy - complemented by the Peng-Robinson (PR) real-gas equation of state (EOS). In the conservation equations, the fluxes of species and heat are written according to fluctuation-dissipation theory [1]. The species fluxes consist of the multicomponent species mass diffusion with a fully populated diffusion matrix and the Soret effect; the heat flux contains the Fourier term, Dufour effects and the enthalpy transported by the species fluxes. All transport properties - viscosity, mass diffusion coefficients, thermal diffusion coefficients and thermal conductivity - are computed using high-pressure-valid mixing rules [13], and thus transport properties are functions of all thermodynamic variables, (p, T, X_α) where T is the temperature and X_α is the mole fraction of species α. The PR EOS is well known to be inaccurate for species other than hydrocarbons and therefore the volume correction of [14] computed from a reference Gibbs free energy is used to enhance its accuracy to the same level as the Lee-Kesler EOS. Details on the entire formulation can be found in [12].

According to the 'alternate approach' suggested by Jordan [15], to obtain the present LES

DNS/ LES	Jet comp.	Chamber comp.	Re_{jet}	Re_{ch}	T_{jet} (K)	T_{ch} (K)	ρ_{jet}/ρ_{ch}
LES	N_2	N_2	1.6×10^5	0	140	298	3.43
DNS	N_2	CO_2	1.0×10^3	0	750	450	0.33

Table 1. Initial conditions and other characteristics of the simulations. The abbreviation "comp." denotes the chemical composition.

conservation equations, the governing differential equations are first transformed into curvilinear coordinates and then filtered with a lowpass filter rather than opposite (i.e. the filtering occurs before the transformation); the two approaches lead to the same mathematical equations. This filtering results in the formation of unclosed terms in the conservation equations that contain the subgrid activity; these are the subgrid-scale (SGS) terms. The LES equations have been presented in general form in [16], and contain the conventional subgrid terms as well as unconventional subgrid terms arising from the steep thermodynamic-variable gradients which are inherent in the flow ([12]). Since LES is only here used in the context of single fluid composition, the unconventional SGS terms identified for a mixture of species initially at different temperatures and the unconventional SGS terms arising from the species fluxes are neglected. Similarly, since the available data is only global, that is, the spatial details of the flow cannot be validated, we also neglect, in a first approximation, the SGS terms arising from the pressure gradient in the momentum equation and the heat flux in the energy equation that were shown to be important to recover in LES the spatial flow details [17, 18]. The constant-coefficient Smagorinsky model is used for the SGS conventional fluxes since it has been shown that if the interest is only in the mean flow, the nature of the SGS model is not as important as the thermodynamics [19].

3. Configuration, numerical method and boundary conditions

The configuration of interest is that of a three-dimensional round jet injected into a chamber at high-p conditions. The chamber dimensions for DNS in the (x_1, x_2, x_3) directions are $25D$, $10D$ and $10D$ respectively where D is the diameter of the jet, here set to be 0.005m. The domain extent for LES are $50D$, $25D$ and $25D$ in the (x_1, x_2, x_3) directions respectively. The domain is large enough to assume that the injected fluid is effectively a free jet. The boundary conditions in the x_2 and x_3 directions are of non-reflecting type for real-gases [20]. In the x_1 axial direction, the boundary conditions are inflow and outflow type. Acoustic reflections due to non–orthogonal wave impingement on the boundaries is prevented by applying sponge boundary conditions [21] and by artificially increasing viscosity near the outflow boundary; this region is not used when presenting statistical averaging results. The jet inflow velocity profile is given by

$$u_1 = \frac{U_j}{2}\left[1 - \tanh\left(\frac{r - r_j}{2\delta}\right)\right] \tag{1}$$

where U_j is the specified jet centerline velocity, $r = \sqrt{x_2^2 + x_3^2}$, r_j is the jet radius and δ is the initial shear layer thickness chosen to be $0.05r_j$. Similar hyperbolic tangent profiles are used at the inflow for the temperature and the species mass fraction. For the DNS, the domain is initialized using a method previously adopted by Nichols et al. [22] for simulating variable density jets at atmospheric pressure. In this method, the same profile as that of the inflow (i.e. $x_1 = 0$) for velocity, temperature and mass fraction is initially specified at all x_1 locations throughout the domain. Random perturbations of amplitude 5% of U_j, in the form of white noise are added to the initial velocity field in the shear layer. After this initial forcing, the flow

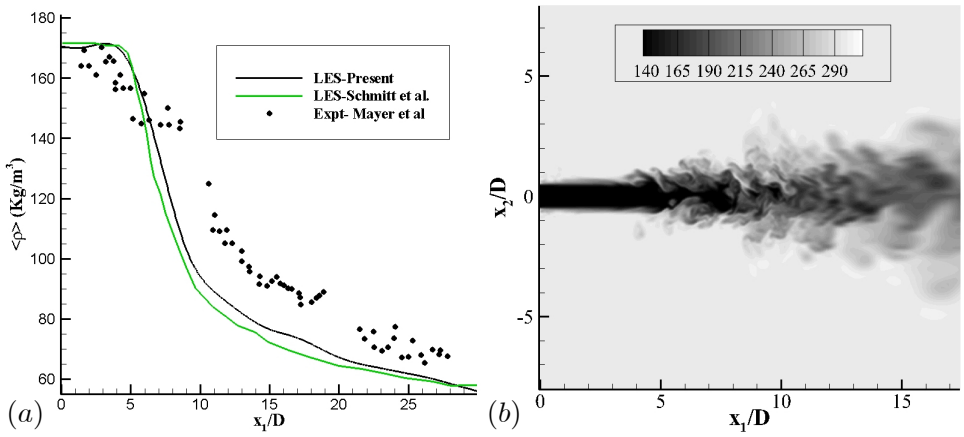

Figure 1. Results from LES of N_2 injection into N_2. (a) Time averaged density variation along jet center line. (b) Instantaneous temperature contours (in K) in the $x_3 = 0$ plane at $t = 0.0416$ s.

evolves with no further perturbations being added. For the LES, the inflow perturbations are provided using the method adopted by Freund [23].

The governing equations are temporally discretized using a fourth-order explicit Runge-Kutta time integration and spatially discretized utilizing a sixth-order compact scheme. In both DNS and LES, stability was achieved by filtering the conservative variables using a tenth-order filter [24]. The filtering was performed every 4 time steps in DNS and every time step in LES; the rationale for these filtering frequencies was explained in detail elsewhere [17].

4. Results

4.1. LES of N_2/N_2 jet

LES of N_2 supercritical jets injected into a chamber containing N_2 were performed in the past. Zong et al. [25] performed two-dimensional jet simulations and compared the radial variation of the density profile at two axial locations to the experimental data of Chehroudi et al. [26]; the agreement with the experimental data was reasonable despite the lack of portraying stretching/tilting effects which are typically considered important in vorticity production. Schmitt et al. [27] performed three-dimensional LES of supercritical jets using a Wall Adapted Local Eddy viscosity(WALE) model and the centerline density profile was compared with the experimental data of Mayer et al. [3] with good agreement. More recently Müller et al. [19] performed LES of Mayer's experiments using the Smagorinsky and Vreman models and found good agreement for the first order statistics between the models and a good agreement with the experiment for the centerline density profile. Considering that different models led to good agreement with data indicates that the data so far available is insufficient to distinguish between, or among, models - a model based on appropriate and relevant physics versus a model containing inappropriate simplifications - and therefore none of the favorable comparisons with available data can be considered a validation of that model. Thus, we propose that good agreement with existing data is only a necessary, but not sufficient condition, for model validation. In fact, we propose that one of the roles of simulations should be to highlight quantities which would constitute discriminating tests able to select the best model to describe high-pressure mixing and combustion.

With the goal of showing the necessary evaluation with the data, LES of a supercritical N_2 jet into a N_2-filled chamber is performed and compared to the experiments of Mayer et al. [3].

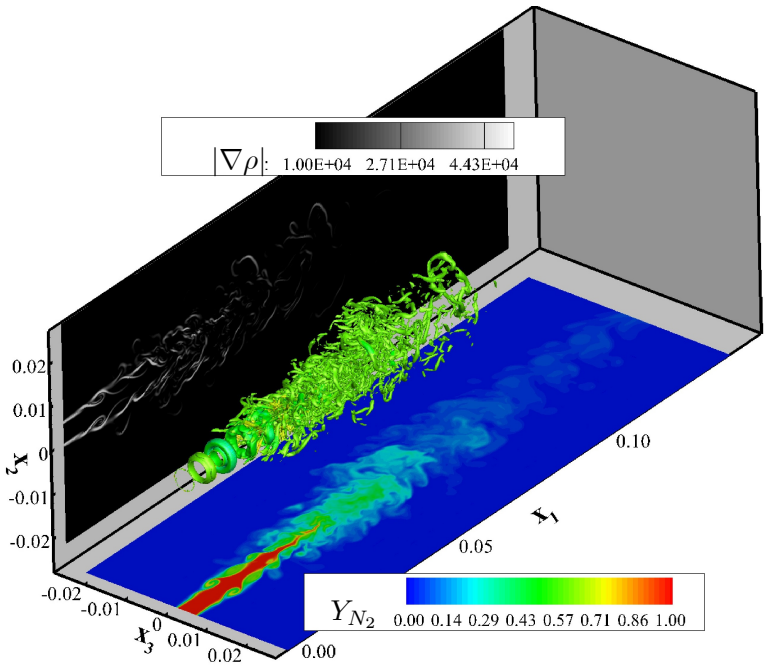

Figure 2. Instantaneous (t = 0.02650 s) results showing isocontours of Q-criterion (in s^{-2}), the second invariant of the velocity gradient tensor, contours of $|\nabla\rho|$ (in kg m^{-4}) in the $x_1 - x_2$ plane and contours of N_2 mass fraction in the $x_1 - x_3$ plane.

The jet exit conditions and chamber conditions are listed in Table 1. Figure 1(a) shows the x_1 variation of the time averaged density along the jet centerline obtained from experiments and simulation. The time averaged quantities (denoted by <> hereafter) is defined over a fixed time interval as

$$< \phi >= \frac{1}{t'} \int_{t_1}^{t_2} \phi(t) dt \tag{2}$$

where $t' = t_2 - t_1$ is the integration time. The jet centerline is defined as the line along which $x_2 = 0$ and $x_3 = 0$, and the values along this line are computed by interpolating from the nodes closest to the line at all x_1 locations. The simulation results agree reasonably with the experimental results. We also compare our results with those of Schmitt et al. [27] and a good agreement is obtained between the two simulations that use very different numerical schemes and turbulence models. This corroborates the observation of Müller et al. [19] that the first order statistics are generally insensitive to the numerical schemes and turbulence models and further reiterates the need for experimental data pertaining to higher order statistics. Figure 1(b) depicts the instantaneous (t = 0.0416 s) temperature contours in the $x_3 = 0$ plane. The presence of small scales downstream of the potential core is evident. Stretched entities emanating from the potential core can be observed that are characteristic of a single-phase mixing layer observed at the edge of supercritical jets.

4.2. DNS of N_2/CO_2 jet

DNS of a supercritical N_2 jet injected into a chamber containing CO_2 is performed at Re_j =1000. To our knowledge, this is the first DNS of a jet having a specified composition that is injected into a chamber having a different composition. The jet exit and chamber conditions are listed in Table 1. Figure 2 shows the isocontours of the Q-criterion which is a commonly used quantity

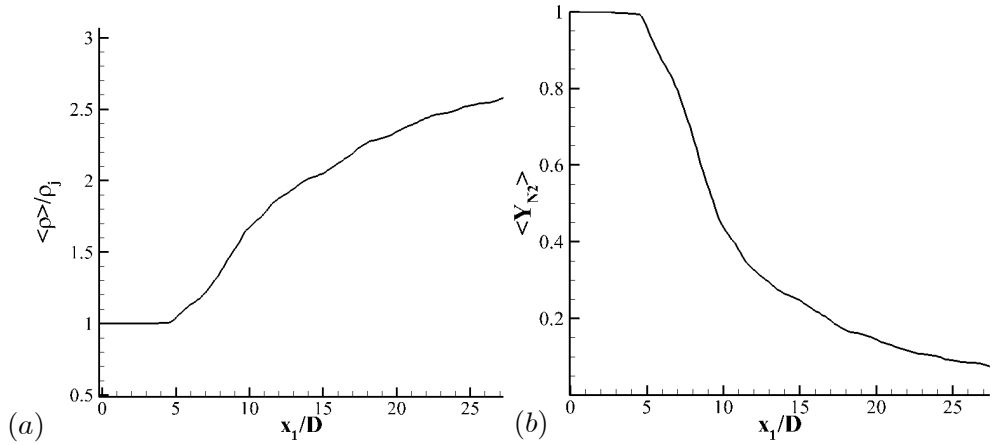

Figure 3. Results from DNS of N_2 injection into CO_2. (a) Time averaged density variation along the jet center line, (b) Time averaged N_2 mass fraction variation along the jet center line.

to visualize vortical structures,

$$Q = \frac{1}{2}\left[\frac{1}{2}\omega_i\omega_i - (S_{ij}S_{ij})\right], \tag{3}$$

where ω_i is the ith component of the vorticity vector and S_{ij} is the strain-rate tensor. The isocontours show the vortex ring near the inflow that further breaks up to produce a range of small scale vortices. Figure 2 shows the $|\nabla\rho|$ contours in the $x_1 - x_2$ plane at $x_3 = 0$. These high-value $|\nabla\rho|$ regions are a significant feature of high-p flows and representing them accurately is an important criterion measuring the success of subgrid scale models in the context of high-p flows. As a manifestation of mixing due to molecular diffusion enhanced by turbulence, shown on the $x_1 - x_3$ plane (at $x_2 = 0$) are the Y_{N_2} contours, $\langle Y_{N_2}\rangle$, where Y is the mass fraction. Since the injected N_2 fluid is lighter than the surrounding, the encountering of the heavier fluid leads to a rapid three-dimensional breakdown of the jet and therefore to enhanced mixing. The edges of mass fraction contours also show evidence of a single-phase mixing layer which is characteristic of supercritical jets, as opposed to spherical droplets formed due to surface tension at subcritical pressures. Quantifying this aspect requires further investigation.

To examine if a potential core exists, statistics are obtained by performing time averaging for approximately $100tU_j/D$. Figure 3(a) shows the variation of $\langle\rho\rangle/\rho_j$ along the jet center line. A time averaged potential core length $x_1/D = 5$ is obtained after which rapid mixing of the jet is observed. Figure 3(b) shows $\langle Y_{N_2}\rangle$ which also exhibits a potential core length that extends 5 diameters downstream of the injector; the decreased $\langle Y_{N_2}\rangle$ past $x_1/D = 5$ is due to mixing with the heavier CO_2 that is responsible for the increase of $\langle\rho\rangle/\rho_j$ past that axial location. To further obtain an understanding of the flow, we investigate time-averaged statistics along the radial direction at four different streamwise locations $x_1/D = 2$, 10, 15 and 20. Figure 4(a) illustrates the variation of the mean axial velocity, non-dimensionalized by the jet centerline velocity, along the radial direction at different streamwise locations. The $x_1/D = 2$ location is inside the potential core and hence the profile retains a shape similar to the inlet velocity profile. However, at further downstream locations, rapid mixing causes the profile to flatten out as the jet fluid mixes with the ambient fluid and the jet spreads out. Figure 4(b) illustrates the variation of $\langle Y_{N_2}\rangle$ along the radial direction. By comparing the mean velocity and mean mass fraction profiles it can be observed that the decay rate of the jet centerline value is larger for the species than that of axial velocity; however the spreading rate in the radial direction

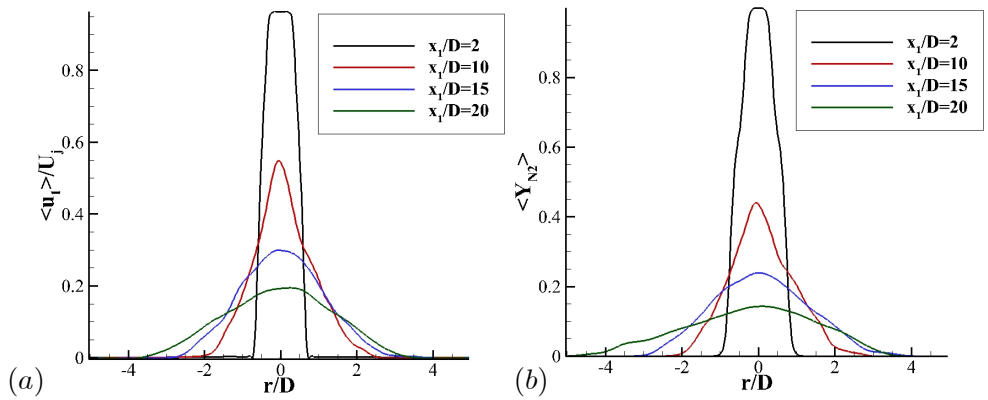

Figure 4. Results from DNS of N_2 injection into CO_2. (a) Variation of time averaged axial velocity (u_1) along the radial direction, (b) Variation of time averaged N_2 mass fraction along the radial direction.

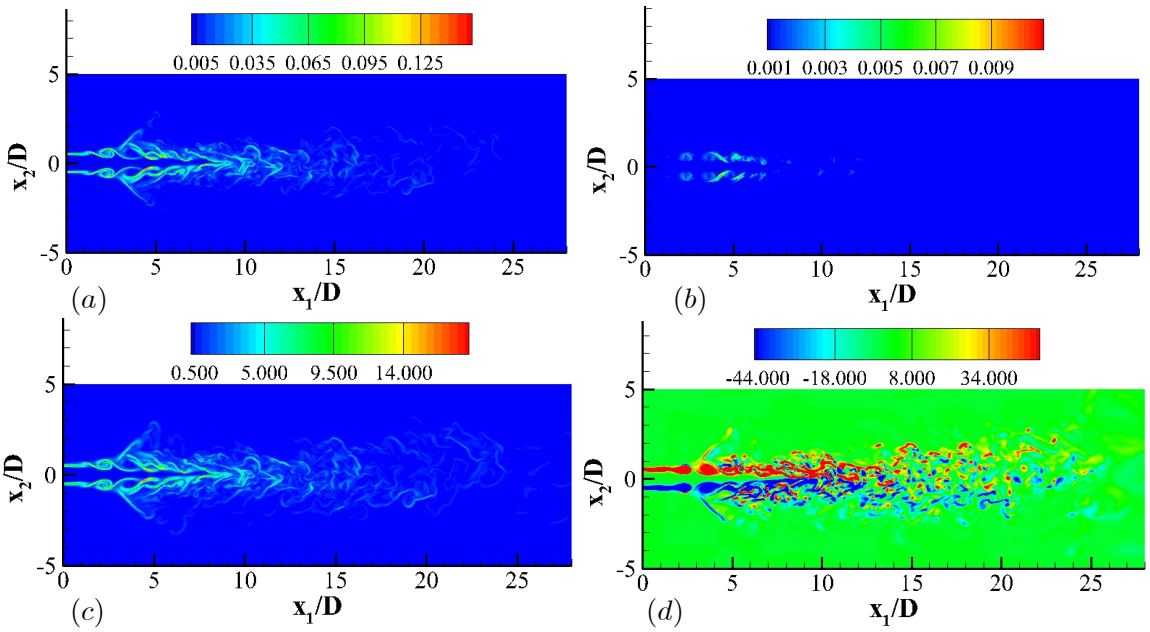

Figure 5. Results from DNS of N_2 injection into CO_2. Species mass flux for CO_2 (a) Contours of $|\rho Y_\alpha D_{T,\alpha} \frac{\nabla T}{T}|$ (kg/s m^2), (b) Contours of $|\rho Y_\alpha D_{p,\alpha} \frac{\nabla p}{p}|$ (kg/s m^2), (c) Contours of $|D'_{\alpha\beta} \frac{m_\alpha}{m_\beta} \nabla Y|$ (kg/s m^2) (d) Contours of ω_3 (s^{-1}). $t = 0.0265$ s.

remains approximately the same. Whether this axial evolution and radial spreading comparison are universal, and if so, the reasons for these effects should be investigated in future work.

At atmospheric p, it is generally considered that mixing occurs primarily due to molecular mass diffusion enhanced by turbulence. Under high-pressure conditions, the Soret effect may also play an important role in species diffusion. The species α mass flux is given by

$$J_{\alpha j} = -\rho \left[Y_\alpha \left(D_{T,\alpha} \right) \frac{1}{T} \frac{\partial T}{\partial x_j} + Y_\alpha \left(D_{p,\alpha} \right) \frac{1}{p} \frac{\partial p}{\partial x_j} + \sum_{\beta=1}^{N-1} \left(D'_{\alpha\beta} \frac{m_\alpha}{m_\beta} \right) \frac{\partial Y_\beta}{\partial x_j} \right] \tag{4}$$

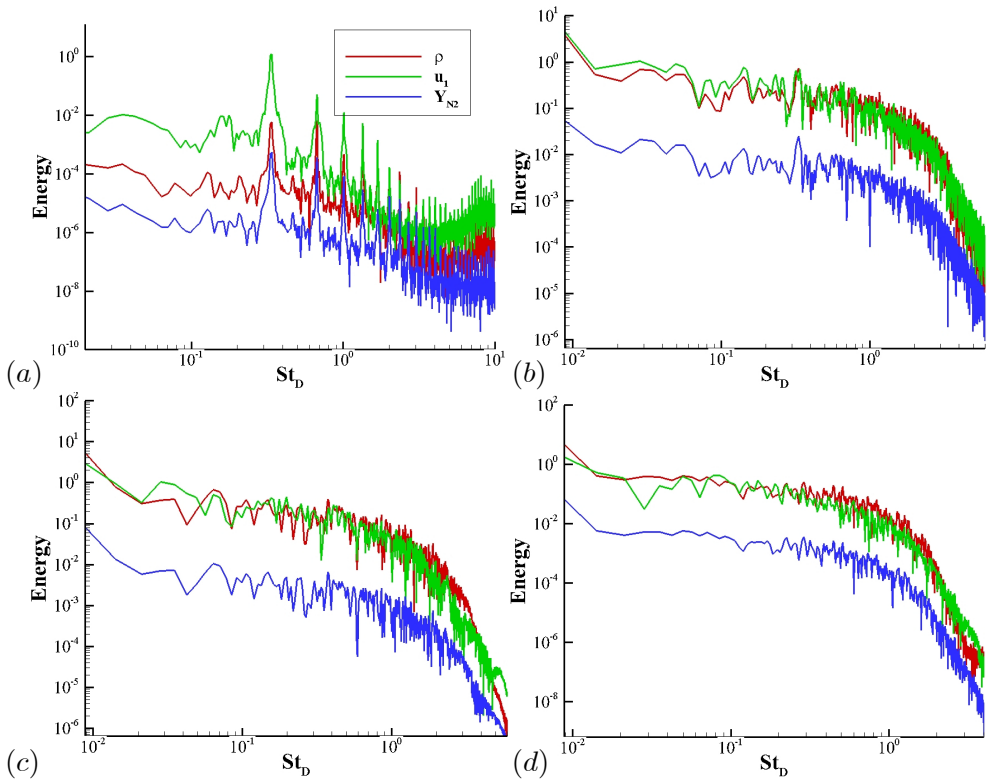

Figure 6. Spectra of ρ, u_1 and Y_{N_2} along the jet center line at $(a) : x_1/D = 4.0$, $(b) : x_1/D = 8.0$, $(c) : x_1/D = 12.0$ and $(d) : x_1/D = 16.0$. The units of Energy (energy spectral density) are JHz^{-1}).

where $D_{T,\alpha}$, $D_{p,\alpha}$ and $D'_{\alpha\beta}$ are diffusion coefficients and m is the molar mass (see [12] for details). The contribution of the Soret term (the first term in Eqn. 4) along with the other two terms are plotted in Figure 5. Since a statistical representation of these terms would involve computing budgets, a calculation which is beyond the scope of this investigation, we defer that calculation to future study and present here only the magnitude of the instantaneous values on $x_3 = 0$ plane. The largest contribution to J_α comes from the mass fraction gradient term (Figure 5(c)) followed by the Soret term (Figure 5(a)) the magnitude of which is approximately two orders of magnitude smaller than the largest term. The contribution of ∇p (Figure 5(b)) is negligible for the current case, as generally accepted. By comparing the spatial distribution of these terms with that of ω_3 contours in Figure 5(d), we can conjecture that these diffusion effects play an important role in the formation of small scales through mixing induced formation of large magnitude $|\nabla\rho|$ regions which act as a solid boundary at which vorticity forms. A detailed evaluation is necessary to further shed light on this aspect. To understand the turbulent characteristics of the flow, a spectral analysis is performed by applying a Fourier transform to ρ, Y_{N_2} and u_1 at four locations ($x_1/D = 4, 8, 12$ and 16) along the jet centerline. A dominant frequency at a Strouhal number ($St_D = fD/U_j$, where f is the frequency ($f = 1/t$)) of 0.33 is obtained. This is the frequency at which a continuous series of vortex rings are generated and is particularly visible as peaks in the spectra at $x_1/D = 4$ in Figure 6(a). As x_1/D increases, (e.g. $x_1/D = 8, 12$ and 16) in Figures 6(b), (c) and (d), the spectra becomes smoother, a fact which is manifestation of a flow with turbulent characteristics. The spectrum shows a monotonic fall in the energy at higher frequencies indicating that all relevant frequencies are captured in the simulation.

5. Summary and Conclusions

Direct Numerical and Large Eddy Simulations are used to study high-pressure jet injection and mixing. LES is first used to evaluate the physical model and numerical method for a cryogenic N_2 jet injected into a N_2-filled chamber. The time averaged density variation along the streamwise direction is compared to the experimental data and a reasonable agreement is obtained therefore fulfilling a necessary condition for suggesting the validity of the physical model and numerical method. The first DNS of a jet of a specified chemical composition injected into a chamber filled with a fluid of different composition is conducted: the DNS is of a supercritical N_2 jet injected into a CO_2-filled chamber. Instantaneous results show that the employed grid and model are able to capture the high density gradient magnitude regions that are characteristic of a high-p flow. The radial variation of mean axial velocity and mean N_2 mass fraction indicate that the centerline decay rate of species concentration is larger than the axial velocity decay rate; whether this fact is universal and its causes will be the subject of future research. The contribution of the Soret term is approximately two orders of magnitude smaller than the mass fraction gradient term; the spatial distribution of all diffusion terms indicate their important role in the formation of smaller turbulent scales. Statistical results show that the mean core length is about $5D$. Spectral analysis shows a dominant frequency of $St_D = 0.33$, the frequency at which vortex rings are produced. Spectra from locations downstream of the potential core show a broadband nature, characteristic of a turbulent flow.

Acknowledgments

This study was conducted at the California Institute of Technology under the sponsorship of the Department of Energy (DoE), Basic Energy Sciences with Drs. Wade Sisk and Mark Pederson as Program Managers and by the Army Research Office with Dr. Ralph Anthenien as Program Manager. Computational time was provided by the NASA Ames Supercomputing Center under the Transformational Tools and Technologies (T3) Project directed by Dr. Michael Rogers and by NERSC under DoE sponsorship.

References

[1] Keizer, J., 1987 *Statistical Thermodynamics of Nonequilibrium Processes* Springler-Verlag, New York.
[2] Oschwald, M. and Schik, A., 1999. Supercritical nitrogen free jet investigated by spontaneous Raman scattering. Experiments in Fluids, 27(6), pp.497-506.
[3] Mayer, W., Tellar, J., Branam, R., Schneider, G. and Hussong, J., 2003 Raman measurements of cryogenic injection at supercritical pressure, Heat and Mass Transfer, 39(8-9), pp. 709-719.
[4] Oschwald, M., Schik, A., Klar, M. and Mayer, W., 1999. Investigation of coaxial LN2/GH2-injection at supercritical pressure by spontaneous Raman scattering. In 35th AIAA/ASME/SAE/ASEE Joint Propulsion Conference and Exhibit.
[5] Chehroudi, B., Talley, D. and Coy, E., 2002. Visual characteristics and initial growth rates of round cryogenic jets at subcritical and supercritical pressures. Physics of Fluids (1994-present), 14(2), pp.850-861.
[6] Segal, C. and Polikhov, S.A., 2008. Subcritical to supercritical mixing. Physics of Fluids (1994-present), 20(5), p.052101.
[7] Roy, A. and Segal, C., 2010. Experimental study of fluid jet mixing at supercritical conditions. Journal of Propulsion and Power, 26(6), pp.1205-1211.
[8] Roy, A., Joly, C. and Segal, C., 2013. Disintegrating supercritical jets in a subcritical environment. Journal of Fluid Mechanics, 717, pp.193-202.
[9] Falgout, Z., Rahm, M., Wang, Z. and Linne, M., 2015. Evidence for supercritical mixing layers in the ECN Spray A. Proceedings of the Combustion Institute, 35(2), pp.1579-1586.
[10] Falgout, Z., Rahm, M., Sedarsky, D. and Linne, M., 2016. Gas/fuel jet interfaces under high pressures and temperatures. Fuel, 168, pp.14-21.
[11] Manin, J., Pickett, L. M. and Crua, C., 2015. Microscopic observation of miscible mixing in sprays at elevated temperatures and pressures. In ILASS meeting, Rayleigh, NC.
[12] Masi, E., Bellan, J., Harstad, K.G. and Okong'o, N.A., 2013. Multi-species turbulent mixing under supercritical-pressure conditions: modelling, direct numerical simulation and analysis revealing species spinodal decomposition. Journal of Fluid Mechanics, 721, pp.578-626.

[13] Harstad, K.G. and Bellan, J., 2004. Mixing rules for multicomponent mixture mass diffusion coefficients and thermal diffusion factors. The Journal of chemical physics, 120(12), pp.5664-5673.
[14] Harstad, K.G., Miller, R.S. and Bellan, J., 1997. Efficient high–pressure state equations. AIChE Journal, 43(6), pp.1605-1610.
[15] Jordan, S.A., 1999. A large-eddy simulation methodology in generalized curvilinear coordinates. Journal of Computational Physics, 148(2), pp.322-340.
[16] Borghesi, G. and Bellan, J., 2015. A priori and a posteriori investigations for developing large eddy simulations of multi-species turbulent mixing under high-pressure conditions, Phys. Fluids, 27, 035117 (35 pages).
[17] Taşkinoğlu, E.S. and Bellan, J., 2010. A posteriori study using a DNS database describing fluid disintegration and binary-species mixing under supercritical pressure: heptane and nitrogen. Journal of Fluid Mechanics, 645, pp.211-254.
[18] Taşkinoğlu, E.S. and Bellan, J., 2011. Subgrid scale models and Large Eddy Simulation of oxygen stream disintegration and mixing with a hydrogen or helium stream at supercritical pressure. Journal of Fluid Mechanics, 679, pp156-193.
[19] Muller, H., Niedermeier, C.A., Matheis, J., Pfitzner, M. and Hickel, S., 2016. Large-eddy simulation of nitrogen injection at trans-and supercritical conditions. Physics of Fluids (1994-present), 28(1), p.015102.
[20] Okong'o, N. and Bellan, J., 2002. Consistent boundary conditions for multicomponent real gas mixtures based on characteristic waves. Journal of Computational Physics, 176(2), pp.330-344.
[21] Bodony, D.J., 2006. Analysis of sponge zones for computational fluid mechanics. Journal of Computational Physics, 212(2), pp.681-702.
[22] Nichols, J.W., Schmid, P.J. and Riley, J.J., 2007. Self-sustained oscillations in variable-density round jets. Journal of Fluid Mechanics, 582, pp.341-376.
[23] Freund, J.B., 2001. Noise sources in a low-Reynolds-number turbulent jet at Mach 0.9. Journal of Fluid Mechanics, 438, pp.277-305.
[24] Kennedy, C.A. and Carpenter, M.H., 1994. Several new numerical methods for compressible shear-layer simulations. Applied Numerical Mathematics, 14(4), pp.397-433.
[25] Zong, N., Meng, S-Y. and Yang, V., 2004 A numerical study of cryogenic fluid injection and mixing under supercritical conditions, Phys. Fluids, 16(12), pp. 4248-4261.
[26] Chehroudi, B., Cohn, R., Talley, D. and Badakhshan, A., 2002 Cryogenic shear layers: Experiment and phenomenological modeling of the initial growth rate undr subcritical and supercritical conditions, Int. J. Heat Fluid Flow, 23, pp. 554-563.
[27] Schmitt, T., Selle, L. Ruiz, A. and Cuenot, B., 2010 Large-eddy simulation of sueprcritical-pressure round jets, AIAA Journal, 48(9), pp. 2133-2144.
[28] Hannoun, I.A., Fernando, H.J.S. and List, E. J., 1988 Turbulence structure near a sharp density interface, J. Fluid Mech. 189, pp. 189-209.